Neighbor of Brca1 gene (Nbr1) functions as a negative regulator of postnatal osteoblastic bone formation and p38 MAPK activity

Caroline A. Whitehouse[a,1], Sarah Waters[a], Katie Marchbank[a], Alan Horner[b], Neil W. A. McGowan[c], Jelena V. Jovanovic[a], Guilherme M. Xavier[c], Takeshi G. Kashima[c], Martyn T. Cobourne[c], Gareth O. Richards[b], Paul T. Sharpe[c], Tim M. Skerry[b], Agamemnon E. Grigoriadis[c,2], and Ellen Solomon[a,2]

[a]King's College London, Department of Medical and Molecular Genetics, London SE1 9RT, United Kindom; [b]Academic Unit of Bone Biology, Section of Musculoskeletal Science, School of Medicine and Biomedical Sciences, Sheffield S10 2RX, United Kingdom; and [c]King's College London, Department of Craniofacial Development and Orthodontics, London SE1 9RT, United Kingdom

Edited by Eric N. Olson, University of Texas Southwestern, Dallas, TX, and approved June 8, 2010 (received for review November 17, 2009)

The neighbor of Brca1 gene (Nbr1) functions as an autophagy receptor involved in targeting ubiquitinated proteins for degradation. It also has a dual role as a scaffold protein to regulate growth-factor receptor and downstream signaling pathways. We show that genetic truncation of murine Nbr1 leads to an age-dependent increase in bone mass and bone mineral density through increased osteoblast differentiation and activity. At 6 mo of age, despite normal body size, homozygous mutant animals ($Nbr1^{tr/tr}$) have ∼50% more bone than littermate controls. Truncated Nbr1 (trNbr1) co-localizes with p62, a structurally similar interacting scaffold protein, and the autophagosome marker LC3 in osteoblasts, but unlike the full-length protein, trNbr1 fails to complex with activated p38 MAPK. $Nbr1^{tr/tr}$ osteoblasts and osteoclasts show increased activation of p38 MAPK, and significantly, pharmacological inhibition of the p38 MAPK pathway in vitro abrogates the increased osteoblast differentiation of $Nbr1^{tr/tr}$ cells. Nbr1 truncation also leads to increased p62 protein expression. We show a role for Nbr1 in bone remodeling, where loss of function leads to perturbation of p62 levels and hyperactivation of p38 MAPK that favors osteoblastogenesis.

bone remodeling | osteoblasts | p62 | autophagy | light chain 3

Postnatal bone development, remodeling, and repair require the precisely coordinated activity of osteoblasts, which produce bone matrix proteins, and osteoclasts, responsible for the removal or resorption of bone. Most acquired systemic bone diseases are caused by aberrant remodeling, where the balance of activities between these cell types is disrupted. Genes that play a key role in the general regulation of the skeleton during both embryonic development and postnatal skeletal remodeling have been identified (reviewed in refs. 1 and 2) and include the neighbor of Breast cancer 1 gene (Nbr1) binding partner p62 (also known as A170/sequestosome 1/orphan nuclear receptor coactivator (ORCA)/lymphocyte-specific protein tyrosine kinase-binding protein (lckBP)) (3). p62 null mice show defects in osteoclastogenesis in vitro because of reduced receptor activator for nuclear factorκ B ligand (RANK-L)–stimulated NF-κB signaling and develop mature-onset obesity and insulin resistance through hyperactivation of ERK and adipogenesis (4).

Nbr1 and p62 are ubiquitously expressed (5, 6). Nbr1 can bind mono- and polyubiquitin (K-63 and K-48 linked) through its C-terminal ubiquitin-associated (UBA) domain (7, 8). In addition to a direct interaction through a common N-terminal Phox and Bem1p (PB1) interaction motif (9), Nbr1 and p62 interact with light chain 3 (LC3) and other autophagy related gene 8 family members involved in the autophagy pathway. This is a potent lysosome-dependent degradation mechanism for the turnover of cytosolic proteins and degradation of bulk cytoplasm, long-lived proteins, organelles, and protein aggregates. Nbr1 and p62 target ubiquitinated substrates to the (macro)autophagosomal pathway (7, 8, 10–12). Mutations of p62 are found in sporadic and 5q35-linked familial cases of Paget's disease of bone (PDB) (13, 14), which is characterized by increased osteoclast and osteoblast activity leading to the formation of an excess of poorly structured bone that is liable to fracture (15, 16). Most p62 mutations identified to date in PDB patients affect the ubiquitin-binding properties of its UBA domain (17), with a biochemical–phenotype correlation existing between ability of mutated protein to bind ubiquitin in vitro and disease severity (17–19).

To investigate the role of Nbr1 in vivo, we disrupted the gene by homologous recombination to produce a truncated protein (trNbr1) lacking the LC3-interacting region (LIR) and UBA domain but containing an intact PB1 domain. We report here that homozygous $Nbr1^{tr/tr}$ mice develop a progressive increase in bone volume and bone mineral density (BMD) because of an increase in the differentiation and activity of bone-forming osteoblasts. The trNbr1 protein can bind p62 and shows overlapping distribution with p62 in punctate LC3-positive autophagosomal vesicles. In vitro culture of $Nbr1^{tr/tr}$ osteoprogenitors showed enhanced p38 MAPK activity, and specific inhibition of p38 MAPK rescued the increased osteoblast differentiation phenotype. These findings provide in vivo evidence that Nbr1 modulates p38 MAPK signaling in osteoblasts and is a regulator of osteoblast differentiation.

Results

Generation of Nbr1-Truncated Mice. Exons 6–8 of *Nbr1* were targeted by homologous recombination in embryonic stem (ES) cells, introducing a stop at codon 135 (Fig. S1 *A–D*). Homozygous $Nbr1^{tr/tr}$ mice were born at the expected Mendelian ratio and grew normally compared with wild-type littermates, with no macroscopic differences in organ morphology or size. Quantitative RT-PCR analysis showed that this targeting strategy did not affect mRNA expression of truncated *Nbr1* or the adjacent *Brca1* gene (5). Protein extracts from $Nbr1^{tr/tr}$ osteoblasts showed loss of the endogenous full-length protein and stable expression of trNbr1 at equivalent levels (Fig. S1*E*).

Increased Bone Mass and BMD in $Nbr1^{tr/tr}$ Mutant Mice. No differences in bone size or dry weight between genotypes at 17.5 days post coitum or in postnatal animals up to 1 mo of age were ob-

Author contributions: C.A.W., M.T.C., P.T.S., T.M.S., A.E.G., and E.S. designed research; C.A.W., S.W., K.M., A.H., N.W.A.M., J.V.J., G.M.X., T.G.K., G.O.R., and A.E.G. performed research; A.E.G. contributed new reagents/analytic tools; C.A.W., S.W., A.H., N.W.A.M., J.V.J., G.O.R., and A.E.G. analyzed data; and C.A.W. and A.E.G. wrote the paper.

The authors declare no conflict of interest.

This article is a PNAS Direct Submission.

Freely available online through the PNAS open access option.

[1]To whom correspondence should be addressed. E-mail: caroline.whitehouse@kcl.ac.uk.

[2]A.E.G and E.S. contributed equally to this work.

This article contains supporting information online at www.pnas.org/lookup/suppl/doi:10.1073/pnas.0913058107/-/DCSupplemental.

DEVELOPMENTAL BIOLOGY

served, but histological analysis of older bones showed a marked increase in bone mass and change in bone architecture in Nbr1$^{tr/tr}$ mice compared with controls (Fig. 1*A*). This increased bone matrix in Nbr1$^{tr/tr}$ mice is of the mature lamellar type and does not show haphazard organization of collagen fibers, a property of woven bone common in PDB (Fig. S2). At 3 mo of age, humeral and femoral widths were increased by 24%, which was maintained at 9 mo of age ($P < 0.01$) (Fig. 1*B*). The increased bone mass was also observed by X-ray analysis, which showed increased radio-opacity, as well as by micro-quantitative computed tomography (μQCT) analysis such that the femoral epiphyses were almost totally ossified by 9 mo of age (Fig. 1 *C* and *D*). Quantification of BMD confirmed a significant increase in cortical and trabecular BMD in femurs and calvariae (Fig. 1*E* and Table S1).

Increased Bone Formation in Nbr1$^{tr/tr}$ Mice. Bone histomorphometric analysis of undecalcified femurs at 2, 6, and 11 mo of age showed significant increases in trabecular bone volume (TBV) and trabecular number (TbN) with a concomitant decrease in mean trabecular separation (MTS) in Nbr1$^{tr/tr}$ mice compared with wild-type mice (Fig. 2 *A*–*C*). Osteoid thickness (OTh) was also increased in Nbr1$^{tr/tr}$ mice (Fig. 2*D*). Interestingly, osteoclast activity was apparently increased in vivo in Nbr1$^{tr/tr}$ mice at 2 mo of age compared with age-matched wild-type mice as measured by histomorphometric parameters of osteoclast surface (OcS) and mean erosion depth (Fig. S3 *A* and *C*), but this seemed to be transient and there were no statistically significant differences in these histomorphometric parameters between the genotypes at either 6 or 11 mo and no differences in eroded surface at any age examined (Fig. S3*B*). Indeed, ex vivo osteoblast-stimulated osteoclast differentiation assays showed no differences in osteoclast number or resorptive activity stimulated by either wild-type or Nbr1$^{tr/tr}$ osteoblasts (Fig. S3*E*). Taken together, these data suggest that the mutant mice might present with some early changes in osteoclast numbers but that this resolves as the mice mature.

Dynamic histomorphometric analysis by double calcein labeling of bone formation over 7 d showed that bone formation rate (BFR) was increased by 41% (at 2 mo) and 61% (at 7 mo) in Nbr1$^{tr/tr}$ mice compared with age-matched controls, indicating increased osteoblast function in young and mature mice (Fig. 2 *E* and *F*). Consistent with these data, levels of osteocalcin, a marker for osteoblastic activity and bone deposition, were shown to be increased in Nbr1$^{tr/tr}$ mice in serum, and this was supported by in situ hybridization studies showing increased osteocalcin expression in Nbr1$^{tr/tr}$ osteoblasts compared with age-matched wild-type femurs (Fig. 2 *G* and *H*). These results suggest that Nbr1 is a negative regulator of osteoblastic bone formation.

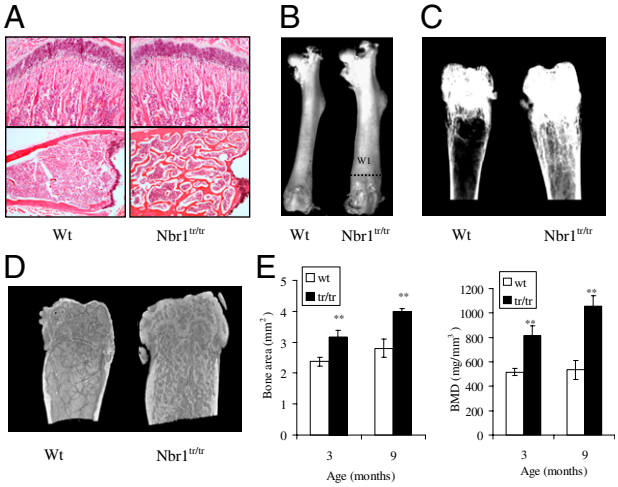

Fig. 1. Increased bone mass and BMD in Nbr1$^{tr/tr}$ mice. (*A*) Histological analysis of femurs from 1-mo-old (*Upper*) and 8-mo-old (*Lower*) wild-type (Wt) and Nbr1$^{tr/tr}$ mice. H&E stain. (*B*) Wt and Nbr1$^{tr/tr}$ femurs of 9-mo-old mice. W1, periosteal width measurement point. (*C*) Radiographs of distal femurs from Wt and Nbr1$^{tr/tr}$ mice at 6 mo of age. (*D*) μQCT images of 12-mo-old Wt and Nbr1$^{tr/tr}$ femurs. (*E*) μQCT analysis of combined femur and cranial bone area and BMD in Nbr1$^{tr/tr}$ and Wt mice aged 3 and 9 mo. Black bars, Nbr1$^{tr/tr}$; white bars, Wt (**$P < 0.01$). Differences between the genotypes were assessed using Student's *t* test; error bars represent SEM ($n = 5$).

Loss of Nbr1 Function Leads to Increased Osteoblast Differentiation and Activity. To further examine the role of Nbr1 in osteoblasts, we first confirmed Nbr1 was expressed in osteoblasts. Semiquantitative RT-PCR analysis showed *Nbr1* RNA present in primary osteoblasts (Fig. 3*A*), and immunohistochemistry analysis confirmed Nbr1 expression in wild-type osteoblasts, which also expressed osteocalcin (Fig. 3 *A* and *B*). To examine the cellular mechanism responsible for the increase in bone mass observed in Nbr1$^{tr/tr}$ mice, we measured osteoprogenitor frequency, proliferation rate, and differentiation capacity in Nbr1$^{tr/tr}$ mice and wild-type controls. Ex vivo cultures of Nbr1$^{tr/tr}$ precursors derived from neonatal calvariae or bone-marrow stromal cells showed significantly increased numbers of osteoprogenitors, with augmented bone nodule numbers, mineralization of bone-forming nodules, and osteogenic colony-forming units (CFU) compared with wild-type controls (Fig. 3 *C* and *D*). The increase in bone mass is not explained by increased proliferation of Nbr1$^{tr/tr}$ osteoblasts compared with wild-type, because the mutant osteoblasts actually grew slightly slower as they reached confluency ($P < 0.05$), although no difference in murine embryonic fibroblast (MEF) proliferation rate was observed (Fig. S4*A*). In accordance with the increased osteoblast differentiation, quantitative RT-PCR analysis showed that the osteoblast marker genes alkaline phosphatase and osteocalcin and the transcription factor Atf4 were elevated ($P < 0.0001$, $P < 0.01$, and $P < 0.01$, respectively) during in vitro osteoblast differentiation at day 15 in Nbr1$^{tr/tr}$ osteoblasts (Fig. 3*E*) and over a time course of differentiation (Fig. S4*B*), whereas levels of the transcription factor CBFA1/Runx2 were unaltered between the genotypes. This is in agreement with the in situ hybridization of osteocalcin being elevated in Nbr1$^{tr/tr}$ femurs (Fig. 2*H*). Taken together, these data suggest that truncation of Nbr1 results in increased bone formation by stimulating osteoblast differentiation and activity.

Nbr1 Regulates p38 MAPK-Dependent Osteoblast Differentiation. Because p62 regulates ERK activity, interacts with p38 MAPK (4), and has been shown to regulate cytokine-dependent p38 MAPK activity (20, 21), we next determined whether Nbr1 truncation, which has an intact p62 binding domain, influenced protein interaction and/or activation of these MAPK pathways. COS-7 cells were transfected with p38 MAPK-myc and either HA-Nbr1 or HA-trNbr1 before stimulation or not with anisomycin to activate p38 MAPK. Whereas full-length Nbr1 was immunoprecipitated with activated p-p38 MAPK, trNbr1 failed to bind to either inactive or active p38 MAPK (Fig. 4*A*). Thus, full-length Nbr1, but not trNbr1, is found in a complex with activated p38 MAPK. Loss of Nbr1–p38 MAPK interaction on Nbr1 truncation suggests that the p38 MAPK pathway may be altered in Nbr1$^{tr/tr}$ cells. Indeed, enhanced p38 MAPK activation was observed in both Nbr1$^{tr/tr}$ osteoblasts and Nbr1$^{tr/tr}$ osteoclast precursors in response to anisomycin or RANK-L treatment (Fig. 4*B* and Fig. S3*D*). Although no consistent increase in ERK phosphorylation was observed in Nbr1$^{tr/tr}$ osteoblasts, increased activation was observed in osteoclasts (Fig. S3*D*). Ex vivo analysis of NF-κB activation (a known downstream pathway of p62) in osteoclasts and MEFs from Nbr1$^{tr/tr}$ mice (Fig. S5 *A* and *B*), canonical Wnt pathway activation in osteoblasts (Fig. S5*C*), and the p38 MAPK downstream effectors heat shock factor protein 1 (HSF1) and heat shock protein 72 (Hsp72) (Fig. S6) did not show significant differences from wild-type cells, suggesting that trunca-

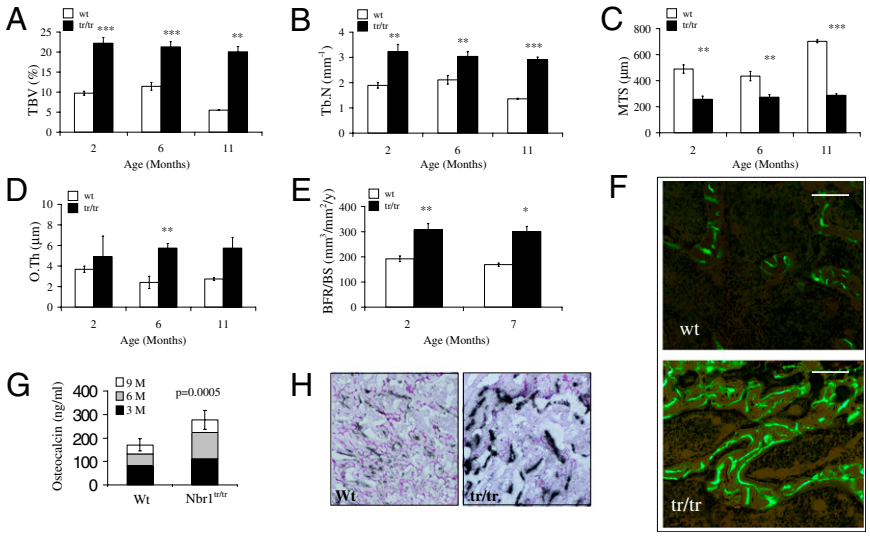

Fig. 2. Histomorphometry analysis of Nbr1$^{tr/tr}$ mice showing an age-dependent increase in bone formation compared with wild-type mice. (*A*) TBV, trabecular bone volume. (*B*) TbN, trabecular number. (*C*) MTS, mean trabecular separation. (*D*) OTh, mean osteoid thickness. (*E*) BFR/BS, bone-formation rate/bone surface. (*$P < 0.05$; **$P < 0.01$, ***$P < 0.001$). Differences between the genotypes were assessed using Student's *t* test. Error bars represent SEM ($n = 3$). (*F*) Calcein double-labeled mineralization fronts in femoral cortex of 8-wk-old mice by fluorescent micrography. (Scale bar, 20 μm.) (*G*) Serum osteocalcin levels in 3- (black bars), 6- (gray bars), and 9-mo-old (white bars) wild-type and Nbr1$^{tr/tr}$ mice ($n = 10$ per group). (*H*) In situ hybridization analysis of osteocalcin mRNA expression in wild-type (Wt) and Nbr1$^{tr/tr}$ (tr/tr) femurs shows elevated expression in Nbr1$^{tr/tr}$ mice. (Magnification: 10×.)

tion of Nbr1 does not affect these particular downstream effectors or pathways.

To examine the extent to which p38 MAPK activation is responsible for the Nbr1$^{tr/tr}$ osteoblast phenotype, we examined the impact of the p38 MAPK inhibitor, SB203580, on the differentiation of wild-type and Nbr1$^{tr/tr}$ calvarial-derived osteoblasts in vitro. Although no effects of SB203580 on cell proliferation or viability were observed, inclusion of the inhibitor reduced Nbr1$^{tr/tr}$ osteoblast differentiation, as measured by alkaline phosphatase and von Kossa staining, to wild-type levels at two concentrations of inhibitor (0.1 and 10 μM) and two incubation periods (4 or 18 d) (Fig. 4*C*). The effect of p38 MAPK inhibition was striking on bone nodule mineralization in both wild-type and Nbr1$^{tr/tr}$ osteoblast cultures, but Nbr1$^{tr/tr}$ osteoblasts still showed enhanced earlier mineralization at day 18 in differentiation medium compared with wild-type cells. Thus, truncation of Nbr1 leads to increased osteoblast differentiation and mineralization through a mechanism involving elevated and prolonged p38 MAPK activity.

trNbr1 Is Localized to LC3-p62–Positive Vesicles and Stabilizes p62. It has been reported that Nbr1 is degraded by autophagy in an LIR-dependent manner (7). We wanted to test whether trNbr1 protein (lacking the LIR and UBA domains but retaining the PB1 domain) was degraded by autophagy, could localize to autophagosomes without the LC3 interacting region, and could still interact with p62. We found that endogenous trNbr1, like full-length protein, is rapidly turned over by autophagy, and only low levels are detectable in the absence of Bafilomycin-A1, an inhibitor of autophagosome processing (Fig. 5*A Top*). trNbr1 also localizes with transfected YFP-LC3 to autophagosomes in osteoblasts (Fig. 5*A*) and co-localizes with endogenous p62 (Fig. 5*B*). These results show that trNbr1 retains localization to p62-positive cytosolic aggregates and LC3-positive autophagosome-like vesicles, probably through heterodimerization with p62, but that this is independent of the LIR of Nbr1 and may be tissue-specific. Although trNbr1 localizes to autophagosomes, it cannot recruit ubiquitinated cargo for degradation through its missing UBA domain. We confirmed that trNbr1 can bind directly to p62 by in vitro GST pull-down assay of in vitro translated HA-p62 (Fig. 5*C*). Recombinant GST-Nbr1 (aa 1–335), including the PB1 and zinc binding (ZZ) domain, and GST-trNbr1 (aa 1–135) both bound in vitro translated HA-p62 at similar levels but not to GST alone. We also show that the GST Nbr1 UBA domain (aa 919–988) itself can bind HA-p62, although not as strongly, and this suggests the possibility that one of the Nbr1 UBA domain cargoes may be p62 itself.

We thus examined the effect of truncation of Nbr1 on endogenous p62 protein levels. As expected, p62 was degraded by autophagy, induced by serum starvation, in both Wt and Nbr1$^{tr/tr}$ cells. However, steady-state levels of p62 were increased in the untreated Nbr1$^{tr/tr}$ cells compared with wild type, suggesting that trNbr1 may stabilize p62 and reduce its normal turnover (Fig. 5*D*).

Discussion

An excess of bone in the skeleton (osteopetrosis or osteosclerosis) can arise from reduced bone resorption, increased new bone formation, or a combination of these two. Although most mouse models with increased bone mass are caused by impaired bone resorption because of defects in osteoclast differentiation or resorption, an increasing number of genes are being identified that regulate osteoblast function in postnatal skeletal remodeling such as *Wnt/LRP5*, *Atf4*, and *Sclerostin* (reviewed in refs. 22 and 23). We now show that truncation of the Nbr1 protein in mice results in an age-dependent increase in bone mass and BMD because of elevated osteoblast activity. The phenotype is of particular significance, because in wild-type mice, bone mass would normally plateau as the animals mature (peak bone mass) and then, decline as they age.

The changes in bone structure and mass are not subtle. We have shown that the effect is predominantly caused by an alteration in osteoblastic function, where even osteoblasts derived from early postnatal animals that have not yet developed an overt skeletal phenotype were able to differentiate and produce significantly increased amounts of bone matrix in vitro compared with controls. These findings were confirmed in older animals where the histomorphometric measurements of osteoblast function are significantly elevated compared with controls and correlate well with the increase in osteoblast differentiation observed in vitro from adult bone-marrow stromal cells. If the effect was solely or predominantly through osteoblasts, then the mice would be expected to mount an increased level of osteoclastic resorption to balance the increased formation, resulting in a normal bone mass and architecture but with a high turnover state. Because their bone mass continues to increase, this is evidence of an alteration in the homeostatic set point for the skeleton in Nbr1$^{tr/tr}$ mice.

The increased osteoblast activity observed in Nbr1$^{tr/tr}$ mice is associated with enhanced activation of the p38 MAPK pathway. Our data supports the view previously put forward by others (24, 25) that p38 MAPK activation can increase osteoblast differentiation, accelerate the final steps of osteoblast maturation, and increase osteoblast-specific gene expression. We were unable to detect a direct interaction between p38 MAPK and Nbr1 by in vitro

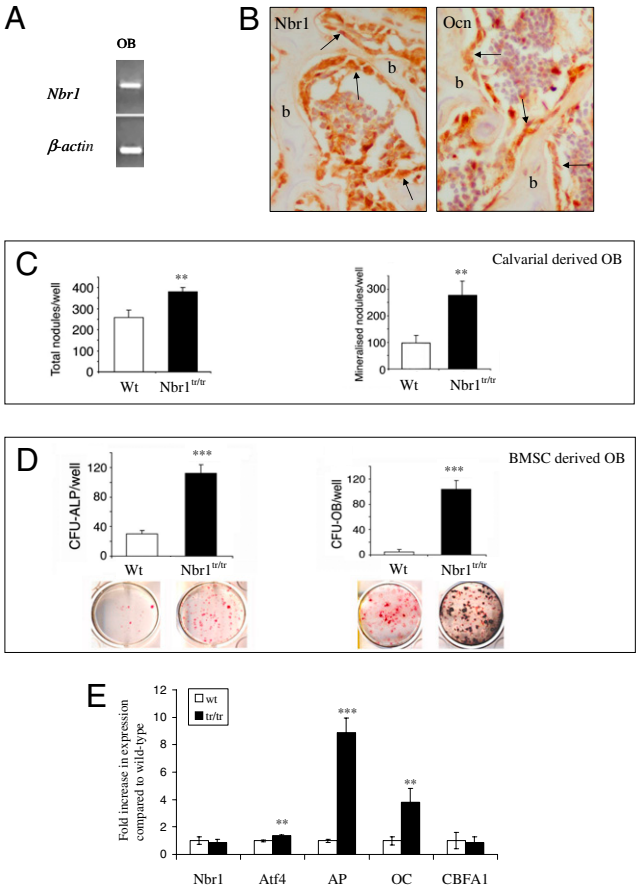

Fig. 3. In vitro characterization of osteoblast differentiation from wild-type (Wt) and Nbr1$^{tr/tr}$ mice. (*A*) RT-PCR analysis confirms endogenous *Nbr1* expression in primary murine osteoblast (OB) cultures. (*B*) Immunohistochemical analysis shows Nbr1 protein expression in osteoblasts (arrows) in 1-mo-old Wt tibiae. Immunohistochemistry on an adjacent section using an osteocalcin (Ocn) antibody confirms the presence of osteoblasts on the surface of bone (b). (*C*) Increased total and mineralized bone-nodule number in primary calvarial OB cultures from Nbr1$^{tr/tr}$ mice compared with Wt. The data represent the mean ± SD of triplicate representative wells (**$P <$ 0.01). (*D*) Increased number of CFU-alkaline phosphatase (CFU-ALP) and CFU-OB from Nbr1$^{tr/tr}$ bone-marrow stromal cells (BMSC) compared with Wt stromal cells [staining: ALP (*Left*); ALP/von Kossa (*Right*)]. The data represent the mean ± SD of six representative wells (***$P < 0.001$). (*E*) Quantitative RT-PCR analysis of OB marker gene expression in calvarial-derived osteoblast cultures from Nbr1$^{tr/tr}$ (black bars) and Wt (white bars) mice at day 15 of osteoblast differentiation showed elevated expression of osteocalcin (OC), Atf4, and alkaline phosphatase (ALP) but not of Nbr1 or CBFA1/Runx2. Relative expression of each gene was normalized to β-actin and levels at day 2, and wild-type expression is set as 1. The data represent the mean ± SD of triplicate wells (**$P < 0.01$; ***$P < 0.001$).

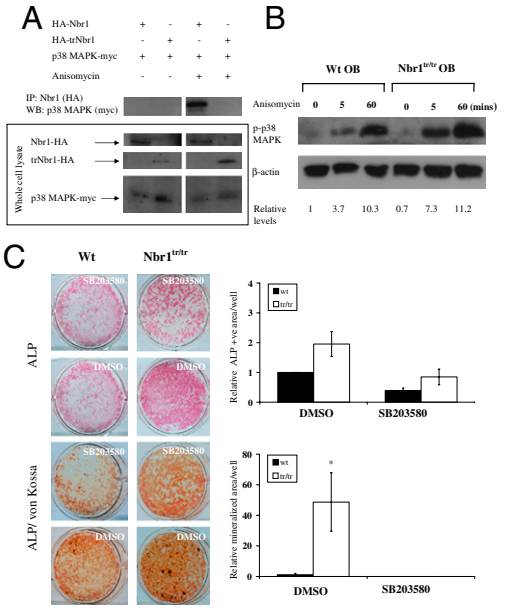

Fig. 4. p38 MAPK activity is increased in Nbr1$^{tr/tr}$ osteoblasts. (*A*) p-p38 MAPK interacts with full-length Nbr1 but not trNbr1. COS-7 cells were transfected with HA-Nbr1, HA-trNbr1, and p38 MAPKmyc constructs for 24 h and stimulated or not stimulated with 5 ng/mL anisomycin for 15 min; extracts were prepared, and co-immunoprecipitation of Nbr1 with p38 MAPK was detected by Western blot analysis. Representative blots of two experiments with similar results are shown. (*B*) Anisomycin-induced p38 MAPK activation in osteoblasts cultured from bone marrow of 3-mo-old Nbr1$^{tr/tr}$ mice is elevated and prolonged compared with Wt cells. (*C*) p38 MAPK inhibition rescues the increased differentiation phenotype in Nbr1$^{tr/tr}$ osteoblasts. Neonatal calvarial-derived osteoblast cultures from Wt or Nbr1$^{tr/tr}$ mice in osteogenic culture for 18 days in the presence of DMSO (vehicle) or 10 μM SB203580 were stained for alkaline phosphatase only [ALP (*Top two rows*)] or ALP followed by von Kossa [ALP/von Kossa (*Bottom two rows*)] and quantified using National Institutes of Health (NIH) Image software. The data represent the mean ± SD of triplicate representative wells normalized to untreated wild-type cells (*$P < 0.05$). Similar results were obtained in the presence of 0.1 μM SB203580.

methods, and we suggest that the interactome complex immunoprecipitated may also include a scaffold for both proteins and that domains deleted in trNbr1 may contribute to the formation of this complex. Inhibition of p38 MAPK with metabolic inhibitors or dominant-negative mutants has been shown to impede osteoblast differentiation. The molecular mechanism behind this control is poorly understood, although it has been suggested that it involves the transcription factor osterix (26). As this manuscript was being prepared, a publication (27) showed that calcium and integrin binding protein (CIB), which we had previously identified as an interacting partner of Nbr1 (28), functions as a Ca^{2+}-sensitive modulator of stress-induced signaling by targeting apoptosis signal-regulating kinase 1 (ASK1), a MAPK kinase kinase in JNK and p38 MAPK signaling pathways, which may fit with the function of Nbr1 in regulating p38 MAPK activity. Furthermore, Nbr1 was recently shown to modulate FGF receptor signaling through interaction with Spred2 (29), and with its previously well-documented involvement in titin kinase signaling in muscle (30), Nbr1 is now becoming recognized as a regulator of diverse cellular kinase signaling pathways.

The trNbr1 protein is lacking several mapped interaction domains, including those for CIB, FEZ1, LC3, USP8, and VTA1/Lip5 (31), which may also have implications for the resulting skeletal phenotype. The loss of the Nbr1 UBA domain described here may also have consequences for the homo- and heterodimerization of Nbr1 and its binding partner p62. We have shown here that the UBA domain of Nbr1 alone can bind p62, suggesting that this may be an additional interaction interface besides the published PB1 domain (3). Homodimerization of p62 through the UBA has been shown to be a regulatory mechanism for directing ubiquitin-binding preferences, where the monomeric UBA is biologically active, binding ubiquitin, whereas the dimeric form precludes ubiquitin binding (32). Dimerization of the UBA domain of the scaffold proteins c-Cbl and Cbl-b and their ubiquitin-binding properties is thought to be a mechanism for regulating the repertoire of downstream signaling through receptor tyrosine kinases. It is not clear what role Nbr1 UBA dimerization has on its ubiquitin binding and signal selectivity.

We have shown that truncation of Nbr1 results in elevated osteoblast differentiation and activity coupled with increased p38

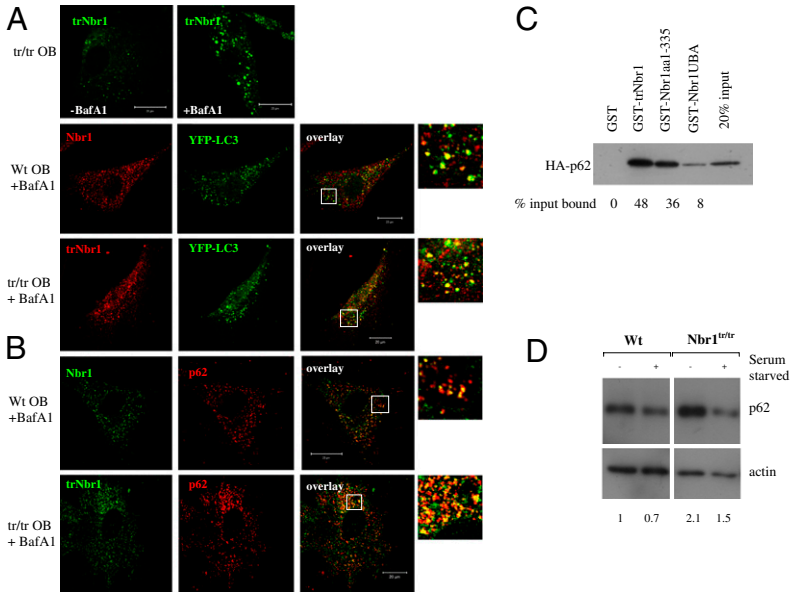

Fig. 5. Effect of Nbr1 truncation on subcellular distribution and p62 levels. (*A Top*) Expression of endogenous trNbr1 increases after 16 h treatment with Bafilomycin-A1 (BafA1) in osteoblasts (OB). (Images were acquired with the same confocal settings). Endogenous Nbr1 and trNbr1 co-localized with transfected YFP-LC3 in murine osteoblasts. (*B*) Endogenous Nbr1 and trNbr1 co-localized with endogenous p62 in murine osteoblasts to autophagosome-like vesicles. (*C*) GST pull-down assays of recombinant GST, GST-trNbr1, GST-Nbr1 aa1-335, and GST-Nbr1UBA aa919-988 with in vitro translated (TnT) HA-p62. Western blot quantification shows that the percentage of input HA-p62 protein bound by GST-trNbr1 and GST-Nbr1aa1-335 are equivalent. (*D*) Representative example of Western blot analysis of p62 in wild-type or $Nbr1^{tr/tr}$ MEFs ± serum starvation for 6 h to induce autophagy to show increased p62 stability in $Nbr1^{tr/tr}$ cells. Actin, loading control. Quantitation of p62 protein is normalized to untreated Wt levels.

MAPK activation. This is in clear contrast to the role of its binding partner, p62 (which shares many structural similarities to Nbr1). Mutations affecting the UBA domain of p62, as found in PDB, are linked to defects not in osteoblast differentiation but in osteoclastogenesis. Our data fit in with perturbation models of human-inherited diseases, where mutations or truncations, rather than complete loss of the gene product, may perturb an interactome and produce a distinct phenotype (33). Nbr1 and p62, therefore, play fundamental roles in the control of bone remodeling through the regulation of signaling pathways in different cell types. However, perhaps more importantly, the identification of the detailed mechanism by which the Nbr1 truncation leads to increased bone mass may be amenable to pharmacological manipulation to increase bone mass in osteoporotic patients.

Experimental Procedures

Generation of *Nbr1* Gene-Targeted Mice. An *Nbr1*-targeting construct as shown in Fig. S1 was electroporated into E14.2 ES cells. After Southern blot screening of 334 clones, two correctly targeted embryonic stem cell clones were microinjected into C57BL/6 blastocysts (B6), and resulting chimeras were mated with B6 mice and backcrossed for 10 generations on the C57BL/6 strain. All studies were approved by the King's College London ethical review committee. Animals were routinely genotyped by PCR using standard conditions, and primer sequences are available on request.

RNA Analysis. RNA was isolated using TRIzol reagent (Gibco-BRL) and relative expression levels determined by quantitative RT-PCR according to standard procedures using the ddCt method, normalized to β-actin and day 2 starting point for each genotype (34). Probe and primer sequences used are available on request.

Bone Morphological, Histological, and in Situ Analyses. Femurs, tibiae, and humeri were isolated and freed of all soft tissue, fixed in 70% ethanol, and dehydrated through graded ethanol before drying at 37 °C until bone weight was stabilized. Bone widths were measured using Mitutoyo 505–628 dial calipers. Radiographic images were obtained using a Faxitron MX-20 Digital Radiography system. Isolated femurs and calvariae were imaged by pQCT with an XCT-μScope (Norland Stratec) using standard procedures. Detailed standard bone histomorphometry was performed on undecalcified femurs collected from age-matched animals at 2, 6, and 11 mo of age ($n = 3$ per time point). For dynamic studies, animals of 2 and 7 mo of age ($n = 3$) were injected with calcein at 30 mg/kg at 7-d intervals, and bones were taken 3 d later. Osteocalcin serum levels was measured using an ELISA immunoassay kit (R&D systems; $n = 10$ per group per time point). For histological and in situ analyses, bones were fixed in 4% paraformaldehyde (PFA), decalcified in 0.5 M EDTA, and processed for paraffin histology; 5-μm sections were stained with H&E. In situ hybridization was carried out using specific Nbr1 and osteocalcin ^{32}P-labeled riboprobes as previously described (35). For immunohistochemistry, specific rabbit polyclonal antibodies against Nbr1 (M. Gautel, King's College London, London) and osteocalcin (sc-30044; Santa Cruz) were used with the Vector ABC staining system and Vector DAB kit (Vector Laboratories) as described previously (36).

In Vitro Differentiation Analyses. Primary osteoblastic cells were isolated from calvariae of 3- to 5-d-old wild-type or $Nbr1^{tr/tr}$ mice using a sequential collagenase digestion protocol described previously (37). For differentiation, cells were cultured in α-minimum essential medium (α-MEM) containing 10% batch-tested FCS (standard medium) and supplemented with 50 μg/mL ascorbic acid and 10 mM sodium β-glycerophosphate (differentiation medium). Cultures were fixed after 15–20 d and stained histochemically for alkaline phosphatase activity or with the von Kossa method for mineralization as described (37). For bone-marrow stromal cell cultures and CFU assays, bone marrow from 3- to 4-mo-old $Nbr1^{tr/tr}$ and wild-type male mice was flushed and cultured in differentiation medium for CFU-ALP and CFU-osteoblast assays in a modification of the method described in ref. 38. The number of CFU-ALP colonies was quantified after alkaline phosphatase staining for 7–9 d, and the number of CFU-OB colonies was quantified after von Kossa staining for 18–21 d. For osteoblast proliferation studies, calvarial-derived osteoblasts or MEFs were plated at a starting density of 5,000 or 10,000 cells per well and counted in triplicate at days 1, 4, and 7 in culture. For osteoblast–osteoclast co-cultures, primary calvarial osteoblasts of the indicated genotype were cultured with macrophage colony stimulating factor –dependent bone-marrow precursors flushed from 9- to 12-wk-old male wild-type and $Nbr1^{tr/tr}$ mice in standard medium containing 10^{-8} M 1,25 α-dihydroxyvitamin D3. Cells were plated on dentine slices, and the number of tartrate resistant acid phosphatase-positive osteoclasts containing three or more nuclei was quantified after 7 d. The percentage resorbed area was quantified after 10 d using a modification of the point-counting method as described in refs. 25 and 39. For p38 MAPK inhibitor assays, calvarial osteoblasts were prepared as described above, and inhibitor was included for either 4 or 18–20 d before alkaline phosphatase and von Kossa staining. Quantification analysis was performed by National Institutes of Health (NIH) Image program (available at http://rsb.info.nih.gov/nih-image/).

Osteoblast Transfection and Immunofluorescence. Neonatal osteoblasts were isolated as described above and transfected using FuGENE 6 (Roche) according to manufacturer's instructions; 24-h posttransfection cells were treated or not treated with 20 μM Bafilomycin-A1 for 16 h before fixation with 4% PFA and staining as described (8). Confocal imaging was performed using a Zeiss LSM510 confocal microscope in sequential scanning mode.

COS-7 Transfection, GST Pull-Down Assays, EMSA, Immunoprecipitation, and Western Blotting. COS-7 cells were cultured in DMEM supplemented with 10%

FCS. Transient transfection of eukaryotic expression vector constructs was performed using FuGENE 6 (Roche), and protein expression or cell treatment was analyzed 24 h later. Cells were treated with 20 μM Bafilomycin-A1 for 16 h or serum starved in DMEM medium for 6 h before cell lysis or treatment with RANK-L or anisomycin at 10 ng/mL and 5 ng/mL, respectively. Protein samples for immunoblotting were prepared from COS-7, MEFs, osteoblast, and osteoclast cultures by extraction in ice-cold lysis buffer (76.5 mM Tris, pH 7.4, 10% glycerol, 2% SDS, 1% Triton X-100) or Immunoprecipitation (IP) buffer [137 mM NaCl, 20 mM Tris, pH 8.0, 0.5% Tween 20, including complete protease inhibitor mixture (Roche) and 1 mM activated sodium orthovanadate]. To confirm protein expression, whole-cell lysates were separated by SDS/PAGE and analyzed by Western blotting. Immunoprecipitations were carried out from precleared cell lysate at 4 °C for 2 h with 2 μg of high-affinity rat anti-HA antibody (Roche) and collected by protein AG agarose beads (Alpha Diagnostic). Beads were washed five times with IP buffer, and bound proteins were eluted by boiling, separated by SDS/PAGE, transferred to PVDF membranes (Immobilon P), probed with the appropriate antibodies, and detected by enhanced chemiluminescence (GE Healthcare) according to manufacturer's instructions. NF-κB EMSA was performed essentially as described in ref. 40. Antibodies used were p38 MAPK, phospho-p38 MAPK, ERK1/2, and phospho-ERK1/2 from Cell Signaling, TRAF6, IK-Bα, NF-κB, HSF1, β-catenin, and myc from Santa Cruz, β-actin from AbCam, Hsp72 from Stressgen, p62 from Abnova, Nbr1 raised against the PB1-ZZ-CC domain or from Abcam, and HA from Roche. Nbr1 GST fusion pull-down experiments were performed essentially as described (8) with GST-Nbr1 recombinant fusion protein expressed and purified from BL21 (DE3) bacterial cells. Equal amounts of recombinant protein were incubated with equal amounts of in vitro transcription/translation-coupled HA-p62 protein (Promega) at 4 °C and washed four times with 20 mM Tris (pH 7.8), 200 mM NaCl, 1 mM EDTA, and 0.5% Nonidet P-40 in the presence of protease inhibitor mixture (Roche). Bound HA-p62 was eluted by boiling the GST beads and then, was separated by SDS/PAGE and immunoblotted for HA-p62.

Statistical Analysis. Statistical analysis was performed by Student's *t* test. For osteocalcin quantification, a mixed-effects model was used to take into account the pseudoreplicates. Fixed effects were age, genotype, and sex, and the response was the natural log of the osteocalcin concentration.

ACKNOWLEDGMENTS. We thank Andrew Stewart (King's College London) and staff in the Biological Services Unit for animal care, Marco Sandri (Venetian Institute of Molecular Medicine, Padua, Italy) for the YFP-LC3 plasmid, Mathias Gautel (King's College London) for helpful discussion and the endogenous Nbr1 polyclonal antibody, David Mangham (Robert Jones and Agnes Hunt Orthopaedic Hospital, Oswestry, UK) for helpful review of the bone pathology, Jennifer Mollon (King's College London) for statistical advice, and members of the E.S. laboratory for reading the manuscript. C.A.W. is supported by an Arthritis Research United Kingdom Fellowship and British Heart Foundation Project Grant, S.W. is supported by Guy's & St Thomas' Charity, J.V.J. is supported by Leukaemia and Lymphoma Research of Great Britain, and K.M. is supported by a Biotechnology and Biological Sciences Research Council (BBSRC) Studentship.

1. Karsenty G, Kronenberg HM, Settembre C (2009) Genetic control of bone formation. *Annu Rev Cell Dev Biol* 25:629–648.
2. Harada S, Rodan GA (2003) Control of osteoblast function and regulation of bone mass. *Nature* 423:349–355.
3. Lamark T, et al. (2003) Interaction codes within the family of mammalian Phox and Bem1p domain-containing proteins. *J Biol Chem* 278:34568–34581.
4. Rodriguez A, et al. (2006) Mature-onset obesity and insulin resistance in mice deficient in the signaling adapter p62. *Cell Metab* 3:211–222.
5. Chambers JA, Solomon E (1996) Isolation of the murine Nbr1 gene adjacent to the murine Brca1 gene. *Genomics* 38:305–313.
6. Joung I, Strominger JL, Shin J (1996) Molecular cloning of a phosphotyrosine-independent ligand of the p56lck SH2 domain. *Proc Natl Acad Sci USA* 93:5991–5995.
7. Kirkin V, et al. (2009) A role for NBR1 in autophagosomal degradation of ubiquitinated substrates. *Mol Cell* 33:505–516.
8. Waters S, Marchbank K, Solomon E, Whitehouse C, Gautel M (2009) Interactions with LC3 and polyubiquitin chains link nbr1 to autophagic protein turnover. *FEBS Lett* 583: 1846–1852.
9. Moscat J, Diaz-Meco MT, Albert A, Campuzano S (2006) Cell signaling and function organized by PB1 domain interactions. *Mol Cell* 23:631–640.
10. Bjørkøy G, et al. (2005) p62/SQSTM1 forms protein aggregates degraded by autophagy and has a protective effect on huntingtin-induced cell death. *J Cell Biol* 171:603–614.
11. Bjørkøy G, Lamark T, Johansen T (2006) p62/SQSTM1: A missing link between protein aggregates and the autophagy machinery. *Autophagy* 2:138–139.
12. Pankiv S, et al. (2007) p62/SQSTM1 binds directly to Atg8/LC3 to facilitate degradation of ubiquitinated protein aggregates by autophagy. *J Biol Chem* 282:24131–24145.
13. Hocking LJ, et al. (2002) Domain-specific mutations in sequestosome 1 (SQSTM1) cause familial and sporadic Paget's disease. *Hum Mol Genet* 11:2735–2739.
14. Laurin N, Brown JP, Morissette J, Raymond V (2002) Recurrent mutation of the gene encoding sequestosome 1 (SQSTM1/p62) in Paget disease of bone. *Am J Hum Genet* 70:1582–1588.
15. Helfrich MH, Hocking LJ (2008) Genetics and aetiology of Pagetic disorders of bone. *Arch Biochem Biophys* 473:172–182.
16. van Staa TP, et al. (2002) Incidence and natural history of Paget's disease of bone in England and Wales. *J Bone Miner Res* 17:465–471.
17. Layfield R, et al. (2006) p62 mutations, ubiquitin recognition and Paget's disease of bone. *Biochem Soc Trans* 34:735–737.
18. Cavey JR, et al. (2005) Loss of ubiquitin-binding associated with Paget's disease of bone p62 (SQSTM1) mutations. *J Bone Miner Res* 20:619–624.
19. Hocking LJ, et al. (2004) Novel UBA domain mutations of SQSTM1 in Paget's disease of bone: Genotype phenotype correlation, functional analysis, and structural consequences. *J Bone Miner Res* 19:1122–1127.
20. Kawai K, Saito A, Sudo T, Osada H (2008) Specific regulation of cytokine-dependent p38 MAP kinase activation by p62/SQSTM1. *J Biochem* 143:765–772.
21. Sugimoto R, et al. (2009) Enhanced neointimal hyperplasia and carotid artery remodeling in sequestosome 1 deficient mice. *J Cell Mol Med*, 10.1111/j.1582-4934.2009.00914.x.
22. Baron R, Rawadi G, Roman-Roman S (2006) Wnt signaling: A key regulator of bone mass. *Curr Top Dev Biol* 76:103–127.
23. Karsenty G (2008) Transcriptional control of skeletogenesis. *Annu Rev Genomics Hum Genet* 9:183–196.
24. Guicheux J, et al. (2003) Activation of p38 mitogen-activated protein kinase and c-Jun-NH2-terminal kinase by BMP-2 and their implication in the stimulation of osteoblastic cell differentiation. *J Bone Miner Res* 18:2060–2068.
25. Gallea S, et al. (2001) Activation of mitogen-activated protein kinase cascades is involved in regulation of bone morphogenetic protein-2-induced osteoblast differentiation in pluripotent C2C12 cells. *Bone* 28:491–498.
26. Wang X, Goh CH, Li B (2007) p38 mitogen-activated protein kinase regulates osteoblast differentiation through osterix. *Endocrinology* 148:1629–1637.
27. Yoon KW, et al. (2009) CIB1 functions as a Ca(2+)-sensitive modulator of stress-induced signaling by targeting ASK1. *Proc Natl Acad Sci USA* 106:17389–17394.
28. Whitehouse C, et al. (2002) NBR1 interacts with fasciculation and elongation protein zeta-1 (FEZ1) and calcium and integrin binding protein (CIB) and shows developmentally restricted expression in the neural tube. *Eur J Biochem* 269:538–545.
29. Mardakheh FK, Yekezare M, Machesky LM, Heath JK (2009) Spred2 interaction with the late endosomal protein NBR1 down-regulates fibroblast growth factor receptor signaling. *J Cell Biol* 187:265–277.
30. Lange S, et al. (2005) The kinase domain of titin controls muscle gene expression and protein turnover. *Science* 308:1599–1603.
31. Rual JF, et al. (2005) Towards a proteome-scale map of the human protein-protein interaction network. *Nature* 437:1173–1178.
32. Long J, et al. (2010) Dimerisation of the UBA domain of p62 inhibits ubiquitin binding and regulates NF-kappaB signalling. *J Mol Biol* 396:178–194.
33. Zhong Q, et al. (2009) Edgetic perturbation models of human inherited disorders. *Mol Syst Biol*, 10.1038/msb.2009.80.
34. Whitehouse C, Chambers J, Catteau A, Solomon E (2004) Brca1 expression is regulated by a bidirectional promoter that is shared by the Nbr1 gene in mouse. *Gene* 326: 87–96.
35. Wilkinson DG, ed (1992) *In Situ Hybridization: A Practical Approach* (IRL, Oxford).
36. Kashima TG, et al. (2009) Periostin, a novel marker of intramembranous ossification, is expressed in fibrous dysplasia and in c-Fos-overexpressing bone lesions. *Hum Pathol* 40:226–237.
37. Harmey D, Stenbeck G, Nobes CD, Lax AJ, Grigoriadis AE (2004) Regulation of osteoblast differentiation by Pasteurella multocida toxin (PMT): A role for Rho GTPase in bone formation. *J Bone Miner Res* 19:661–670.
38. Oreffo RO, Virdi AS, Triffitt JT (1997) Modulation of osteogenesis and adipogenesis by human serum in human bone marrow cultures. *Eur J Cell Biol* 74:251–261.
39. Grigoriadis AE, Heersche JN, Aubin JE (1996) Analysis of chondroprogenitor frequency and cartilage differentiation in a novel family of clonal chondrogenic rat cell lines. *Differentiation* 60:299–307.
40. Yeh WC, et al. (1997) Early lethality, functional NF-kappaB activation, and increased sensitivity to TNF-induced cell death in TRAF2-deficient mice. *Immunity* 7:715–725.